THE FAST STEEPEST DESCENT PATH ALGORITHM FOR ANALYZING SCATTERING FROM TWO-DIMENSIONAL OBJECTS †

E. Michielssen and W. C. Chew

Center for Computational Electromagnetics
Electromagnetics Laboratory
Department of Electrical and Computer Engineering
University of Illinois at Urbana-Champaign
Urbana, IL 61801

Abstract

A novel algorithm for accelerating the iterative solution of integral equations governing scattering from surfaces is presented. The proposed Fast Steepest Descent Path Algorithm (FASDPA) complements previously developed fast solvers, notably the Fast Multipole Method (FMM) and the Matrix Decomposition Algorithm (MDA). Whereas the computational complexity per iteration of a two-level FMM and MDA is $O(N^{3/2})$, the FASDPA permits a matrix-vector multiply in $O(N^{4/3})$ operations.

† This work was supported in part by the University of Illinois Research Board, the National Science Foundation under grant ECS-9502138, the Office of Naval Research under grant N00014-95-1-0872, and the National Science Foundation under grant NSF ECS 93-02145. This paper was published in *Radio Science*, vol. 31, no. 5, pp. 1215-1224, Sept-Oct 1996.

Filename: fsdpa1.tex, Date:October 19, 1996

1. Introduction

Recently, the electromagnetics community has shown a renewed interest in iterative solvers as a means for solving very large scattering problems. A number of techniques have been proposed that permit fast matrix-vector multiplications of matrices that arise in the Method of Moments (MoM) solution of such problems. These techniques may drastically reduce the computational cost associated with the iterative solution of large scattering problems. Examples include, but are not limited to, the Impedance Matrix Localization (IML) technique [Canning, 1993; Canning 1990], the Complex Multipole Beam Approach (CMBA) [Boag et al., 1994], the Fast Multipole Method (FMM) [Coifman et al., 1993], the Matrix Decomposition Algorithm [Michielssen and Boag, 1994], the Adaptive Integral Method (AIM) and pre-corrected FFT method [Bleszynski et al., 1994; White et al., 1994; Phillips and White, 1994]. Both the IML and the CMBA rely on forming directive radiation beams by using special basis and testing functions, and are limited in scope to scattering by sufficiently smooth bodies. The FMM, MDA and the AIM rely on a multilevel geometrical partitioning of the scatterer, and on an expansion of the scattered fields in terms of plane waves and equivalent sources, respectively, and are applicable to the analysis of arbitrarily shaped scatterers. When used in conjunction with an iterative solver, the cost per iteration of the two-level implementations of the FMM and the MDA scales as $O(N^{1.5})$. Recently, multilevel versions of the FMM (MLFMA) [Lu and Chew, 1994; Song and Chew, 1995] and the MDA (MLMDA) [Michielssen and Boag, 1994; Michielssen and Boag, 1995] have been developed. The cost per iteration of these algorithms scales as $O(N \log N)$ and $O(N \log^2 N)$, respectively.

Whereas multilevel algorithms asymptotically exhibit the lowest possible computational cost, they are typically outperformed by two-level algorithms for problems involving medium size scatterers. This is especially true for two-dimensional problems. The proposed Fast Steepest Descent Path Algorithm (FASDPA) constitutes a novel two-level algorithm that hybridizes the FMM and the MDA. Not unlike the FMM and the MDA, the FASDPA starts from a spatial decomposition of the scatterer into a large number of subscatterers, and interactions between nearby subscatterers are accounted for directly. Interactions between distant subscatterers are expressed in terms of a small set of equivalent sources that exhaust the degrees of freedom of the interaction field, as in the MDA. To permit the algorithm to "recycle" information in a manner similar to the FMM, the field radiated by each group is represented in terms of a set of homogeneous plane waves. Equivalent source amplitudes are obtained from the plane wave spectrum. The computational complexity of the FASDPA is $O(N^{4/3})$ per iteration without proceeding to a multi-level scheme.

This paper is organized as follows. Section 2 outlines the proposed FASDPA. Sections 3 describes numerical results obtained using this solver for perfectly conducting scatterers. Finally, Section 4 outlines conclusions and suggestions for future work.

2. Formulation

This section outlines the proposed Fast Steepest Descent Path Algorithm (FASDPA). The scattering problem under consideration is discussed in Section 2.1. Single stage versions of the Fast Multipole Method (FMM) and the Matrix Decomposition Algorithm (MDA) are reviewed in Section 2.2. The FASDPA, which hybridizes the FMM and MDA, and which results in a further reduction of the computational complexity, is introduced in Section 2.3.

2.1. General Formulation

Consider the two-dimensional (2D) perfect electrically conducting (p.e.c.) surface scatterer S depicted in Figure 1. The scatterer is illuminated by a TM_z field $\mathbf{E}(\boldsymbol{\rho}) = \hat{z}E_z^{inc}(\boldsymbol{\rho})$. Throughout this paper, a the time dependence $e^{-i\omega t}$ is assumed and suppressed. The scattered field can be described in terms of the current $J_z(\boldsymbol{\rho})$ residing on S. By enforcing the total electric field along S to vanish, an Electric Field Integral Equation (EFIE) in terms of

$J_z(\boldsymbol{\rho})$ is obtained:

$$\frac{ik\eta}{4}\int_s dS' g(\boldsymbol{\rho}-\boldsymbol{\rho}')\mathbf{J}_z(\boldsymbol{\rho}') = -E_z^{inc}(\boldsymbol{\rho}), \quad \forall \boldsymbol{\rho} \in S \tag{1}$$

where $k = \omega\sqrt{\mu_0\epsilon_0}$ and $\eta = \sqrt{\mu_0/\epsilon_0}$ denote the wave-number and the free-space impedance, respectively, and $g(\boldsymbol{\rho}-\boldsymbol{\rho}') = H_0^{(1)}(k|\boldsymbol{\rho}-\boldsymbol{\rho}'|)$. This EFIE is often solved through discretization using the Method of Moments (MoM). S is approximated by N straight segments of width Δ_j, $j = 1, \cdots, N$. The current on each segment is assumed constant and given by $\tilde{I}_j$, $j = 1, \cdots, N$, i.e.,

$$\mathbf{J}_z(\boldsymbol{\rho}) = \sum_{j=1}^{N} \tilde{I}_j p_j(\boldsymbol{\rho}) \tag{2}$$

where $p_j(\boldsymbol{\rho})$ represents a unit pulse function residing on segment j. Substituting Equation (2) into (1), and enforcing the resulting equation at the centers of the segments $\boldsymbol{\rho}_i$, $i = 1, \cdots, N$, results in a system of linear equations in the unknown expansion coefficients $\tilde{I}_j$, $j = 1, \cdots, N$:

$$\overline{\mathbf{Z}} \cdot \mathbf{I} = \mathbf{V} \tag{3}$$

Approximate expressions for the elements of $\overline{\mathbf{Z}}$ are [Harrington, 1968]

$$Z_{ij} = \begin{cases} 1 + \frac{2i}{\pi}\ln\left[\frac{\gamma k \Delta_j}{4e}\right], & i = j \\ H_0^{(1)}(k\rho_{ji}), & i \neq j \end{cases} \tag{4}$$

where $\rho_{ji} = |\boldsymbol{\rho}_{ji}|$, $\boldsymbol{\rho}_{ji} = \boldsymbol{\rho}_i - \boldsymbol{\rho}_j$, and γ is the Euler's constant. The elements of $\mathbf{V}$ and $\mathbf{I}$ are given by

$$V_i = -E_z^{inc}(\boldsymbol{\rho}_i) \tag{5}$$

$$I_i = \frac{k\eta\Delta_i}{4}\tilde{I}_i \tag{6}$$

The computation of the MoM matrix $\overline{\mathbf{Z}}$ requires $O(N^2)$ operations. The solution of Equation (3) using an iterative solver, e.g., CG or QMR, requires one to repetitively multiply $\overline{\mathbf{Z}}$ by a trial solution vector $\mathbf{I}_q$, at a cost of $O(N^2)$ per iteration if this operation is performed by a direct multiplication. These costs typically prohibit the solution of large scattering problems.

2.2. The Fast Multipole Method and the Matrix Decomposition Algorithm

Recently, a number of techniques have been developed that accelerate the iterative solution of Equation (3) by expediting the required matrix-vector multiply. Two such algorithms, namely the FMM and the MDA, are reviewed in this section.

To apply the FMM to the analysis of scattering from S, the latter is decomposed into L subscatterers denoted by S^I, $I = 1, \cdots, L$. The FMM relies on a reduced representation of the $\overline{\mathbf{Z}}$ matrix given by:

$$\overline{\mathbf{Z}} = \overline{\mathbf{Z}}_{NF} + \overline{\mathbf{Z}}_{FF} \tag{7}$$

where $\overline{\mathbf{Z}}_{FF}$ is further decomposed as

$$\overline{\mathbf{Z}}_{FF} = \overline{\mathbf{V}}^t \cdot \overline{\mathbf{T}} \cdot \mathbf{V} \tag{8}$$

In (7-8) $\overline{\mathbf{Z}}_{NF}$, $\overline{\mathbf{T}}$ and $\overline{\mathbf{V}}$ are all sparse matrices, and superscript "t" denotes a transpose. It is assumed that the groups are approximately of equal size, i.e., that each group contains approximately $M = N/L$ current sources. Given the decomposition of the scatterer into subscatterers, all matrices can be block-decomposed accordingly. For example, $\overline{\mathbf{Z}}^{IJ}$ denotes the submatrix of $\overline{\mathbf{Z}}$ describing the electric field at observation points on S^I due to current elements residing on section S^J. Near-field interactions are defined as interactions between neighboring subsections and self-interactions. $\overline{\mathbf{Z}}_{NF}$ contains these entries of the original $\overline{\mathbf{Z}}$ matrix that describe near-field interactions, i.e., $\overline{\mathbf{Z}}_{NF}^{IJ} = \overline{\mathbf{Z}}^{IJ}$ if sections S^I and S^J reside in each other's immediate vicinity, otherwise $\overline{\mathbf{Z}}_{NF}^{IJ} = \overline{0}$.

The product $\overline{\mathbf{Z}}_{FF} = \overline{\mathbf{V}}^t \cdot \overline{\mathbf{T}} \cdot \mathbf{V}$ represents all far-field interactions. $\overline{\mathbf{V}}$ is block diagonal, i.e., $\overline{\mathbf{V}} = diag[\overline{\mathbf{V}}^1, \overline{\mathbf{V}}^2, \cdots, \overline{\mathbf{V}}^L]$. Each matrix $\overline{\mathbf{V}}^I$ permits the construction of the "far-field pattern" associated with the currents residing on the corresponding subsection S^I, by sampling the pattern in Q directions given by

$$\alpha_q = \frac{2\pi(q-1)}{Q} \tag{9}$$

To ensure accuracy, the Q angles should sample the far-field pattern at the Nyquist rate, and therefore $Q \propto M$. Hence, the elements of the $Q \times M$ matrix $\overline{\mathbf{V}}^I$ are given by

$$V_{qi}^I = e^{i\mathbf{k}_q \cdot \boldsymbol{\rho}_{i_I c_I}} \tag{10}$$

where $\mathbf{k}_q = k(\hat{\mathbf{x}} \cos\alpha_q + \hat{\mathbf{y}} \sin\alpha_q)$, and $\boldsymbol{\rho}_{i_I c_I} = \boldsymbol{\rho}_{c_I} - \boldsymbol{\rho}_{i_I}$ where $\boldsymbol{\rho}_{c_I}$ and $\boldsymbol{\rho}_{i_I}$ denote the center and the ith source associated with group I, respectively (Figure 2).

Given the far-field pattern of each group, far-field group interactions are described by the translation matrix $\overline{\mathbf{T}}$. The FMM derives its name from the fact that the $Q \times Q$ submatrices $\overline{\mathbf{T}}^{IJ}$ are diagonal. In the original FMM, $\overline{\mathbf{T}}^{IJ}$'s entries are given by

$$\begin{aligned} T_{qq'}^{IJ} &= \sum_{p=-Q/2}^{Q/2} H_p^{(1)}(k\rho_{c_J c_I}) e^{-ip(\phi_{c_J c_I} - \alpha_q - \pi/2)}, \qquad && q = q' \\ &= 0, && q \neq q', \end{aligned} \tag{11}$$

where $H_p^{(1)}(\cdot)$ is the pth-order Hankel function on the first kind, and $\phi_{c_J c_I}$ is the angle associated with the vector $\boldsymbol{\rho}_{c_J c_I} = \boldsymbol{\rho}_{c_I} - \boldsymbol{\rho}_{c_J}$. It is easily verified that submatrices $\overline{\mathbf{Z}}^{IJ}$ describing far-field interactions can be expressed as

$$\overline{\mathbf{Z}}_{FF}^{IJ} = \left(\overline{\mathbf{V}}^I\right)^t \cdot \overline{\mathbf{T}}^{IJ} \cdot \overline{\mathbf{V}}^J. \tag{12}$$

It should be noted that, when multiplying the MoM matrix by a vector, explicit use should be made of Equation (8), since multiplying each submatrix separately using (12) does not lead to a reduced computational complexity. In other words, the reduced computational complexity of the FMM is due to the fact that the FMM recycles radiation spectra of all the subscatterers.

The total cost associated with multiplying $\overline{\mathbf{Z}}$ by a trial solution vector is given by

$$C^{FMM} = C_{\overline{\mathbf{Z}}_{NF}} + C_{\overline{\mathbf{Z}}_{FF}}^{FMM}, \tag{13}$$

where $C_{\overline{\mathbf{Z}}_{NF}}$ and $C_{\overline{\mathbf{Z}}_{FF}}^{FMM}$ represent the computational costs associated with multiplying $\overline{\mathbf{Z}}_{NF}$ and $\overline{\mathbf{Z}}_{FF}$ by a vector using the FMM, respectively. The latter can be decomposed as $C_{\overline{\mathbf{Z}}_{FF}}^{FMM} = C_{\overline{\mathbf{V}},\overline{\mathbf{V}}^t} + C_{\overline{\mathbf{T}}}$. These costs are proportional to

$$C_{\overline{\mathbf{Z}}_{NF}} \propto LM^2 \tag{14}$$

$$C_{\overline{\mathbf{V}},\overline{\mathbf{V}}^t} \propto LQM \tag{15}$$

$$C_{\overline{\mathbf{T}}} \propto L^2 Q \tag{16}$$

Since $L = N/M$, and $Q \propto M$, the cost C^{FMM} is minimized provided that $M \propto N^{1/2}$. Under these conditions, $C^{FMM} \propto N^{3/2}$.

The MDA constitutes a different algorithms for accelerating a matrix-vector multiply in the iterative solution of MoM problems. Like the FMM, the MDA relies on a judicious decomposition of the MoM impedance matrix. However, when compared to the FMM, the MDA exploits totally different and complementary properties of the MoM matrix. Just like the FMM, the MDA calls for a decomposition of the scatterer into a large number of subscatterers. Also, as in the FMM, near-field submatrices are stored explicitly in $\overline{\mathbf{Z}}_{NF}$ (7). To efficiently represent far-field interactions, i.e., to decompose $\overline{\mathbf{Z}}_{FF}$, the MDA relies on the fact that the electromagnetic field, radiated by currents residing over a finite-size source region, and observed over a finite observation domain, is characterized by a limited number of Degrees of Freedom (DoF). A simple argument based on the sampling theorem suggests that the number of DoF of the scattered field is proportional to the extent of the source and observation regions, and inversely proportional to the distance separating both regions [Francia, 1956]. A refined analysis [Francia, 1969; Bucci and Franceschetti, 1989] based on the theory of prolate harmonics, reveals that the number of DoF in the scattered field can be determined safely by using the sampling theorem.

In the MoM-based analysis of scattering problems, the limited number of DoF of the fields scattered by objects of finite size reflects itself in the rank-deficiency of the far-field submatrices $\overline{\mathbf{Z}}^{IJ}$. In other words, the fields observed over subscatterer S^I due to the M sources residing on subscatterer S^J do not constitute a linearly independent set. As a result, these fields can be approximated in terms of those radiated by a far smaller set of equivalent sources, in a number equal to the number of DoF, $DoF(I,J)$, describing the interaction between S^I and S^J. A rigorous theory can be formulated if the locations of these $DoF(I,J)$ equivalent sources are selected such that they span a surface enclosing the source region. Let $\boldsymbol{\rho}_{j_{J_e}}$, $j = 1, \cdots, DoF(I,J)$ denote the locations of the equivalent sources associated with the source region, and let $\boldsymbol{\rho}_{i_{I_e}}$, $i = 1, \cdots, DoF(I,J)$ denote a similar set of points on a surface bounding the observation region (Figure 3). It then can be shown that the far field submatrices $\overline{\mathbf{Z}}^{IJ}$ can be expressed as a product of low rank matrices as

$$\overline{\mathbf{Z}}_{FF}^{IJ} = \overline{\mathbf{Z}}^{IJ_e} \cdot [\overline{\mathbf{Z}}^{I_eJ_e}]^{\dagger} \cdot \overline{\mathbf{Z}}^{I_eJ} \tag{17}$$

where $\dagger$ denotes a Moore-Penrose (pseudo-) inverse [Golub and Van Loan, 1991], and $\overline{\mathbf{Z}}^{IJ_e}$, $\overline{\mathbf{Z}}^{I_eJ_e}$, and $\overline{\mathbf{Z}}^{I_eJ}$ are $M \times DoF(I,J)$, $DoF(I,J) \times DoF(I,J)$, and $DoF(I,J) \times M$ matrices describing the interactions between the (equivalent) sources and observation points associated with subscatterers I and J, respectively, i.e.,

$$\begin{aligned}
\overline{\mathbf{Z}}_{ij}^{IJ_e} &= H_0^{(1)}(k|\boldsymbol{\rho}_{i_I} - \boldsymbol{\rho}_{j_{J_e}}|), \\
\overline{\mathbf{Z}}_{ij}^{I_eJ_e} &= H_0^{(1)}(k|\boldsymbol{\rho}_{i_{I_e}} - \boldsymbol{\rho}_{j_{J_e}}|), \\
\overline{\mathbf{Z}}_{ij}^{I_eJ} &= H_0^{(1)}(k|\boldsymbol{\rho}_{i_{I_e}} - \boldsymbol{\rho}_{j_J}|).
\end{aligned} \tag{18}$$

The number of DoF describing the interaction between subsections I and J, $DoF(I,J)$, is proportional to the dimensions of both subsections I and J, i.e., M^2, and inversely proportional to the distance between the subsections,

$|I-J|M$, and bounded from below by a constant, i.e.,

$$DoF(I,J) \propto \frac{M^2}{|I-J|M} + C = \frac{M}{|I-J|} + C. \tag{19}$$

During the iterative solution of the MoM matrix equation, all far-field submatrices $\overline{\mathbf{Z}}^{IJ}$ are multiplied by a vector independently of each other; hence, in contrast to the FMM, the MDA does not recycle information to attain a reduced computational complexity.

The computational cost of the MDA is given by

$$C^{MDA} = C_{\overline{\mathbf{Z}}_{NF}} + C^{MDA}_{\overline{\mathbf{Z}}_{FF}} \tag{20}$$

where $C^{MDA}_{\overline{\mathbf{Z}}_{FF}}$ represents the cost of independently multiplying all far-field submatrices using Equation (17), and can be computed as

$$\begin{aligned} C^{MDA}_{\overline{\mathbf{Z}}_{FF}} \propto & \sum_I M \left[\sum_J DoF(I,J) \right] \\ \propto & \sum_I M \left[M + \frac{M}{2} + \cdots + \frac{M}{L} + LC \right] \\ \propto & LM \left[M + \frac{M}{2} + \cdots + \frac{M}{L} + LC \right] \\ \propto & LM^2 \ln L + L^2 M, \end{aligned} \tag{21}$$

The cost per iteration is again minimized if $M \propto N^{1/2}$. Under those assumptions, $C^{MDA} \propto N^{1.5} \ln N$.

2.3. The Fast Steepest Descent Path Algorithm (FASDPA).

In view of the complementary nature of the FMM and the MDA, these algorithms can be hybridized into an even faster algorithm. The resulting FASDPA has a complexity of $O(N^{4/3})$ per iteration. It should be noted that previously developed two-stage algorithms, notably the Ray Propagation Fast Multipole Algorithm (RPFMA) developed by Wagner and Chew [Wagner and Chew, 1994], and a similar algorithm suggested by Coifman, Rohklin and Wandzura [Coifman et al., 1994], achieve the same complexity. These algorithms take advantage of the fact that Equation (10) represents a Fourier series that has beam-forming characteristics. These beam-forming characteristics can be enhanced by choosing other windows with a smooth roll-off, e.g., cosine tapered functions, which result in a $\overline{\mathbf{T}}^{IJ}$ with only few diagonal entries as plane waves not traveling in the direction $\boldsymbol{\phi}_{c_J c_I}$ are observed to not contribute significantly.

The FASDPA relies on a different technique for accelerating the evaluation of the far-field contribution to the scattered field. Using an integral representation of the zeroth order Hankel function, a far-field matrix element can be expressed as [Chew, 1990]

$$\begin{aligned} Z_{ij}^{IJ} =& H_0^{(1)}(k\rho_{j_J i_I}) \\ =& \frac{1}{\pi}\int d\alpha\, e^{i\mathbf{k}(\alpha)\cdot\boldsymbol{\rho}_{j_J i_I}} \end{aligned} \tag{22}$$

where $\mathbf{k}(\alpha) = k(\hat{\mathbf{x}}\sin\alpha + \hat{\mathbf{y}}\cos\alpha)$, and the integration is over a suitably chosen path in the complex plane. Using $\boldsymbol{\rho}_{j_J i_I} = \boldsymbol{\rho}_{c_I i_I} + \boldsymbol{\rho}_{c_J c_I} + \boldsymbol{\rho}_{j_J c_J}$, we may express the above integral also as (Figure 4)

$$H_0^{(1)}(k\boldsymbol{\rho}_{ji}^{JI}) = \frac{1}{\pi}\int d\alpha\, e^{i\mathbf{k}(\alpha)\cdot\boldsymbol{\rho}_{c_I i_I}} e^{i\mathbf{k}(\alpha)\cdot\boldsymbol{\rho}_{c_J c_I}} e^{i\mathbf{k}(\alpha)\cdot\boldsymbol{\rho}_{j_J c_J}} \tag{23}$$

This integral can be evaluated by choosing an integration path SDP_{JI}, defined in terms of the real and imaginary parts of $\alpha = \alpha_R + i\alpha_I$ as

$$SDP_{JI}: \quad \cos\left(\alpha_R + \phi_{c_J c_I} + \frac{\pi}{2}\right)\cosh(\alpha_I) = 1 \tag{24}$$

SDP_{JI} corresponds to the steepest descent path of the integrand in (22) provided that $\boldsymbol{\rho}_{c_I i_J} = \boldsymbol{\rho}_{j_J c_J} = 0$. The stationary phase or saddle point is at $\alpha = \frac{\pi}{2} - \phi_{c_J c_I}$. Even if this condition does not hold true, it is easily verified that accurate knowledge of the far-field due to a source is only required in the interval

$$\frac{\pi}{2} - \phi_{c_J c_I} - BW < \alpha < \frac{\pi}{2} - \phi_{c_J c_I} + BW \tag{25}$$

where $BW = D/\rho_{c_J c_I}$ is the angle covered by S^I as seen from S^J (D represents the maximum radius of all groups). Outside of this interval, the exponential decay associated with $e^{i\mathbf{k}(\alpha)\cdot\boldsymbol{\rho}_{c_J c_I}}$ renders the integrand negligible along SDP_{JI}. Because of the band limited nature of the far-field pattern function, the number of degrees of freedom within this interval is fixed and given by $DoF(I,J) \propto 2kBW$ [Bucci and Francescetti, 1989].

To arrive at a fast multiplication algorithm, the far-field patterns of both groups are approximated in terms of those associated with $DoF(I,J)$ equivalent sources as:

$$\begin{aligned} e^{i\mathbf{k}(\alpha)\cdot\boldsymbol{\rho}_{j_J c_J}} &\simeq \sum_{l=1,DoF(I,J)} c_l^J e^{i\mathbf{k}(\alpha)\cdot\boldsymbol{\rho}_{l_{J_e} c_J}} \\ e^{i\mathbf{k}(\alpha)\cdot\boldsymbol{\rho}_{c_I i_I}} &\simeq \sum_{l=1,DoF(I,J)} c_l^I e^{i\mathbf{k}(\alpha)\cdot\boldsymbol{\rho}_{c_I l_{I_e}}} \end{aligned} \tag{26}$$

To determine the coefficients c_l^J in (26), the far-field radiated by the source at $\boldsymbol{\rho}_{j_J}$ is matched to that radiated by the $DoF(I,J)$ equivalent sources in the $DoF(I,J)$ directions adjacent to $\phi_{c_J c_I}$. Denoting these directions as α_{q_l}, $l = 1,\cdots,DoF(I,J)$, the vector $\mathbf{c}^J$ containing the coefficients c_l^J, $l = 1,\cdots,DoF(I,J)$ is seen to be the solution to

$$\overline{\mathbf{V}}^J_{\{q_l\},i} = \overline{\mathbf{F}}^{IJ} \cdot \mathbf{c}^J, \tag{27}$$

where $\overline{\mathbf{V}}^J_{\{q_l\},i}$ contains a subset of the i-th column of $\overline{\mathbf{V}}^J$ containing the entries corresponding to all directions α_{q_l}, and $F_{li}^{IJ} = e^{i\mathbf{k}_{q_l}\cdot(\boldsymbol{\rho}_{c_I} - \boldsymbol{\rho}_{i_{I_e}})}$. Alternatively, and perhaps more rigorously, one can interpolate the far-field pattern of a source group, e.g., using approximate prolate harmonics [Bucci and Francescetti, 1989], and match the interpolated far-field pattern to that produced by the equivalent sources along the SDP.

Substituting (26) into (23) and making use of (22) yields

$$\begin{aligned} H_0^{(1)}(k\boldsymbol{\rho}_{j_J i_I}) &= \sum_{l=1,DoF(I,J)} \sum_{l'=1,DoF(I,J)} c_l^I c_{l'}^J H_0^{(1)}(k\boldsymbol{\rho}_{l_{J_e} l'_{I_e}}) \\ &= \left(\mathbf{c}^I\right)^t \cdot \overline{\mathbf{Z}}^{I_e J_e} \cdot \mathbf{c}^J \end{aligned} \tag{28}$$

Noting that $\mathbf{F}^{IJ}$ can be used for all source points, and performing a similar operation for all the receivers, we may finally express a far-field submatrix $\overline{\mathbf{Z}}_{FF}^{IJ}$ as

$$\overline{\mathbf{Z}}_{FF}^{IJ} = \left(\overline{\mathbf{V}}^{I}\right)^{t} \cdot \tilde{\overline{\mathbf{T}}}^{IJ} \overline{\mathbf{V}}^{J} \tag{29}$$

In contrast FMM's $\overline{\mathbf{T}}^{IJ}$, the FASDPA's $\tilde{\overline{\mathbf{T}}}^{IJ}$ is not diagonal. As illustrated in Figure 4, $\tilde{\overline{\mathbf{T}}}^{IJ}$ is empty except for the $DoF(I,J) \times DoF(I,J)$ translation block $\left[F^{IJ}\right]^{\dagger t} \cdot \overline{\mathbf{Z}}^{I_e J_e} \cdot \left[F^{IJ}\right]^{\dagger}$ appearing on the diagonal.

The computational cost per multiplication of the FASDPA can be expressed as

$$C^{FASDPA} = C_{\overline{\mathbf{Z}}_{NF}} + C_{\overline{\mathbf{Z}}_{FF}}^{FASDPA} \tag{30}$$

where $C_{\overline{\mathbf{Z}}_{FF}}^{FASDPA} = C_{\overline{\mathbf{V}},\overline{\mathbf{V}}'} + C_{\tilde{\overline{\mathbf{T}}}}$. The cost $C_{\tilde{\overline{\mathbf{T}}}}$ of multiplying $\tilde{\overline{\mathbf{T}}}$ by a vector is

$$\begin{aligned}
C_{\tilde{\overline{\mathbf{T}}}} =& \sum_{I}\sum_{J} \left(DoF(I,J)\right)^2 \\
\propto& \sum_{I}\sum_{J} \left[\frac{M}{|I-J|} + C\right]^2 \\
\propto& \sum_{I}\sum_{J} \left[\frac{M^2}{|I-J|^2} + \frac{2MC}{|I-J|} + C^2\right]^2 \\
\propto& L(M^2 + 2CM \ln L + LC^2) \\
\propto& LM^2 + 2CML \ln L + L^2C^2.
\end{aligned} \tag{31}$$

Substituting (31) into (30), ignoring the $\ln L$ dependence, and minimizing the total cost w.r.t. M, yields an optimal group size of $M \propto N^{1/3}$. The overall cost per iteration becomes $C^{FASDPA} \propto N^{4/3} \ln N$. It can be shown that the C^{FASDPA} can be further reduced to $C^{FASDPA} \propto N^{4/3}$ if the FMM is used to describe interactions between groups for which $D^2/\rho_{c_J c_I} > 1$, and the above described hybrid FMM-MDA for all other groups. Therefore, the FASDPA will outperform a single stage FMM for large problems. Since both the FMM and MDA can be made accurate to arbitrary precision, so can the FASDPA since it constitutes a hybrid of both.

3. Numerical Results

This section will present a variety of numerical results that illustrate the usefulness of the above described FASDPA.

First, consider a planar strip of length $L = 100\ \lambda$, illuminated by a normally incident plane wave. The bistatic RCS of this strip computed using the FASDPA is shown in Figure 5 and compared to the RCS obtained using a direct solver. Both results are in perfect agreement.

Next, consider the finite sinusoidal grating depicted in the inset in Figure 6. The grating has a length L =12,000 λ, and the periodicity and height of the profile are $P = 8\ \lambda$ and $H = 1\ \lambda$, respectively. The grating is illuminated by a normally incident plane wave. The magnitude of the current excited on the structure, near its left edge, is shown in Figure 6. The results obtained using the FASDPA are in agreement with those obtained using a fast direct solver for planar and elongated structures developed earlier by our group [Michielssen et al., 1995]. Figure 7 depicts the bistatic RCS of the structure. Again, the FASDPA results coincide with those obtained using the fast direct solver.

Figure 8 shows the bistatic RCS of a 2D corner reflector, each side of which measures 639 λ. The structure is modeled in terms of N=12,800 unknowns. Results obtained using the FASDPA are seen to be in good agreement with those obtained using the aforementioned MLMDA [Michielssen and Boag, 1994; Michielssen and Boag, 1995].

The corrugated semicircle of radius r depicted in the inset of Figure 9 was analyzed next. The periodicity of the triangular corrugations equals $p = 1.57$ λ, their depth is $d = 0.5\ \lambda$, and the structure is illuminated by a TM_z plane wave traveling along the $\phi = 0$ direction. Figure 9 shows the bistatic RCS of this structure for $r = 9\ \lambda$ and $r = 639\ \lambda$ (N =25,600). The bistatic RCS of the $r = 9\ \lambda$ structure compares very well with that obtained using a traditional MoM formulation, and the RCS of the $r = 639\ \lambda$ structure compares reasonably well to that obtained using the MLMDA.

To verify our claims regarding the computational complexity of FASDPA, scattering from the finite grating structure of Figure 6 was analyzed for various L, by varying N from N =1,024 upto N =32,826. CPU-times per iteration for the FASDPA are compared to data for the MDA and MLMDA (All programs were ran on a SUN SPARC 20) in Figure 10. Measured CPU-times per iteration closely adhere to the theoretical $O(N^{3/2} \log N)$ (MDA), $O(N^{4/3} \log N)$ (FASDPA) and $O(N \log^2 N)$ (MLMDA) trends. The FASDPA appears to outperform the MDA if $N > 10,000$, and the MLMDA appears to outperform the FASDPA if N >30,000.

4. Conclusions

This paper introduced the FASDPA, a novel technique for accelerating the iterative solution of integral equations for surface scatterers. The FASDPA hybridizes the previously developed FMM and MDA. The computational complexity and memory requirements of the algorithm outlined in this paper are $O(N^{4/3} \ln N)$ and can be further reduced to $O(N^{4/3})$ in a straightforward manner. Starting from an integral representation of the appropriate Green's function, the FASDPA constructs a reduced representation of the interaction field between subscatterers by expressing the integrand in terms of a limited set of functions which permit a closed form evaluation of the integral. The interaction field is described in terms of a small set of discrete sources, and their excitation coefficients are recovered from the plane wave spectrum of a group. The FASDPA was applied to the analysis of TM_z scattering from two-dimensional perfectly conducting scatterers, and results obtained using the FASDPA agree very well with those obtained using other techniques.

In the past, closed-form Green's functions for stratified media have been developed with a view to accelerating the analysis of layered media problems [Aksun and Mittra, 1992]. These techniques rely on the expansion of Sommerfeld integrands in terms of sets of functions which permit a closed-form evaluation of the Sommerfeld integral in terms of a finite set of discrete sources. We anticipate that FASDPA-based algorithms equipped with closed form Green's functions for layered media, can be applied to the analysis of scattering and radiation from objects residing a multilayered background as well. This, and three-dimensional implementations of the FASDPA, are the next focus of our research.

References

[1] M. I. Aksun and R. Mittra, "Derivation of closed-form Green's function for a general microstrip geometry," *IEEE Trans. Microwave Theory Tech.*, vol. 40, pp. 2055- 2062, 1992.

[2] E. Bleszynski, M. Bleszynski, and T. Jaroszewicz, "A fast integral-equation solver for electromagnetic scattering problems," in *IEEE Int. Conf. AP-S*, pp. 416-419, 1994, Seattle, WA.

[3] A. Boag, E. Michielssen, and R. Mittra, "Hybrid multipole beam approach to electromagnetic scattering problems," *Journal of the Applied Computational Electromagnetics Society*, vol. 9, pp. 7-17, 1994.

[4] O. M. Bucci and G. Franceschetti, "On the degrees of freedom of scattered fields," *IEEE Trans. Antennas Propagat.*, vol. 37, pp. 918-926, 1989.

[5] F. X. Canning, "A new combined field integral equation for impedance matrix localization (IML)," in *IEEE-AP/S International Symposium*, pp. 1140-1143, 1993, Ann Arbor.

[6] F. X. Canning, "Transformations that produce a sparse moment method matrix," *J. Electromag. Waves Appl.*, vol. 4, pp. 903-913, 1990.

[7] W. C. Chew, *Waves and Fields in Inhomogeneous Media*, 1990, New York: Van Nostrand Reinhold, pp. 453-469.

[8] R. Coifman, V. Rohklin, and S. Wandzura, "Faster single-stage multipole method for the wave equation," in *10th Annual Review of Progress in Applied Computational Electromagnetics*, pp. 19-24, 1994, Monterey.

[9] R. Coifman, V. Rohklin, and S. Wandzura, "The fast multipole method for the wave equation: a pedestrian prescription," *IEEE Ant. Propag. Mag.*, vol. 35, pp. 7-12, 1993.

[10] G. T. D. Francia, "Degrees of Freedom of an Image," *J. Opt. Soc. Am.*, vol. 59, pp. 779-804, 1969.

[11] G. T. D. Francia, "Directivity, super-gain and information," *IRE Transactions on Antennas and Propagation*, vol. 4, pp. 473-478, 1956.

[12] G. Golub, and L. Van Loan, *Matrix Computations*, 1991, The Johns Hopkins University Press, p. 642.

[13] R. F. Harrington, *Field Computation by Moment Methods*, 1968, Robert E. Krieger Publishing Company, Inc., p. 229.

[14] C. C. Lu and W. C. Chew, "A multilevel algorithm for solving a boundary integral equation of wave scattering," *Micr. Opt. Tech. Lett.*, vol. 7, pp. 456-461, 1994.

[15] E. Michielssen and A. Boag, "A multilevel matrix decomposition algorithm for analyzing scattering from large structures," in *11th Annual Review of Progress in Applied Computational Electromagnetics*, pp. 614-620, 1995, Monterey.

[16] E. Michielssen and A. Boag, "Multilevel evaluation of electromagnetic fields for the rapid solution of scattering problems," *Microwave and Optical Technology Letters*, vol. 7, pp. 790-795, 1994.

[17] E. Michielssen, A. Boag, and W. Chew, "Scattering from elongated structures: direct solution on $O(Nlog^2(N))$ operations," in *1995 International Symposium on Electromagnetic Theory*, pp. 464-468, 1995, St. Petersburg, Russia.

[18] J. Phillips and J. White, "A precorrected FFT method for capacitance extraction of complicated 3-D structures," in *Proceedings of the Int. Conf. on Computer-Aided Design*, pp. November 1994, Santa Clara, California.

[19] J. M. Song and W. C. Chew, "Multilevel fast multipole algorithm for solving combined field integral equation of electromagnetic scattering," *Mico. Opt. Tech. Lett.*, vol. 10, pp. 14-19, 1995.

[20] R. L. Wagner and W. C. Chew, "A ray-propagation fast multipole algorithm," *Micr. Opt. Tech. Lett*, vol. July 1994, pp. 435-438, 1994.

[21] J. White, J. R. Phillips, and T. Korsmeyer, "Comparing precorrected FFT and fast multipole algorithms for solving three dimensional potential problems," in *Proc. of the Colorado Conference on Iterative Methods*, pp. April 1994, Breckenridge, Colorado.

Figure Captions

Figure 1. Perfectly conducting scatterer S subdivided into subscatterers S^I, $I = 1, \cdots, L$, illuminated by a TM_z plane wave $\mathbf{E}(\boldsymbol{\rho}) = \hat{z}E_z^{inc}(\boldsymbol{\rho})$.

Figure 2. Set of groups (I, J), and FMM-based decomposition of $\overline{\mathbf{Z}}_{FF}$.

Figure 3. Set of groups (I, J), and MDA-based decomposition of $\overline{\mathbf{Z}}_{FF}^{IJ}$.

Figure 4. Set of groups (I, J), and FASDPA-based decomposition of $\overline{\mathbf{Z}}_{FF}$. In the FASDPA, the submatrices $\tilde{\overline{\overline{\mathbf{T}}}}^{IJ}$ are not diagonal but contain a small dense block.

Figure 5. Bistatic RCS of a strip scatterer.

Figure 6. Current on a finite corrugated profile.

Figure 7. Bistatic RCS of a truncated corrugated profile shown in Figure 6.

Figure 8. Bistatic RCS of an L-profile.

Figure 9. Bistatic RCS of a corrugated semi-circle.

Figure 10. Comparison of CPU-times per iteration for MDA, FASDPA, and MLMDA.

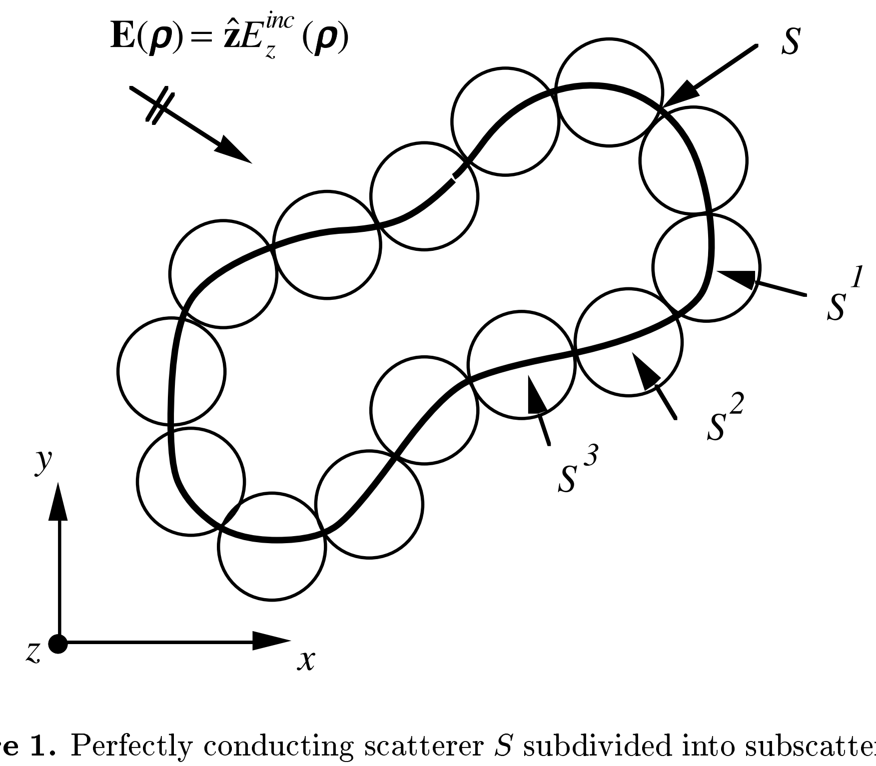

Figure 1. Perfectly conducting scatterer S subdivided into subscatterers S^I, $I = 1, \cdots, L$, illuminated by a TM_z plane wave $\mathbf{E}(\boldsymbol{\rho}) = \hat{z}E_z^{inc}(\boldsymbol{\rho})$.

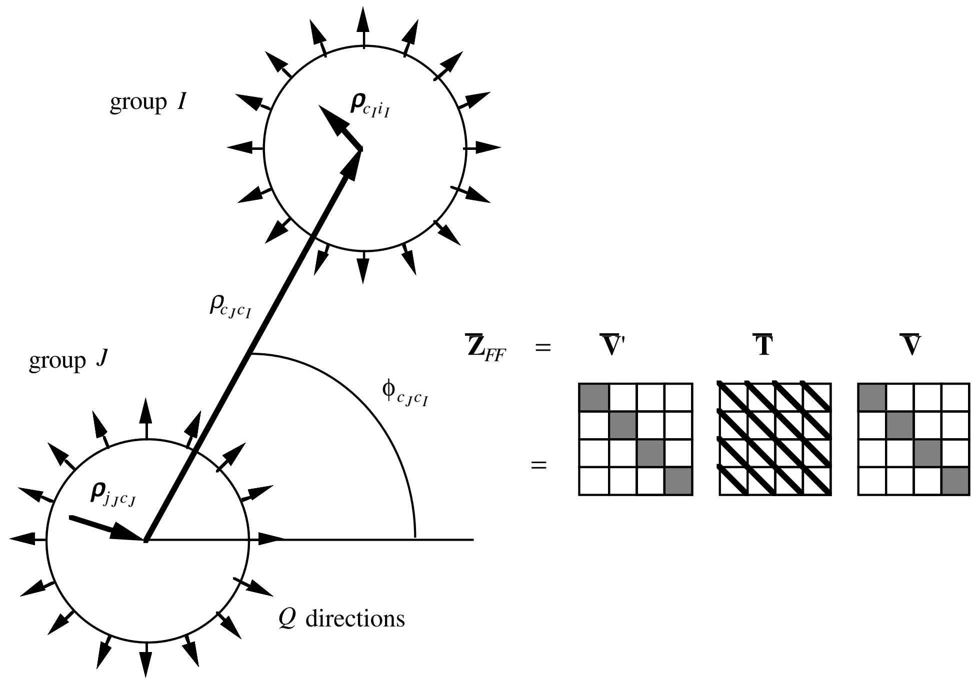

Figure 2. Set of groups (I, J), and FMM-based decomposition of $\overline{\mathbf{Z}}_{FF}$.

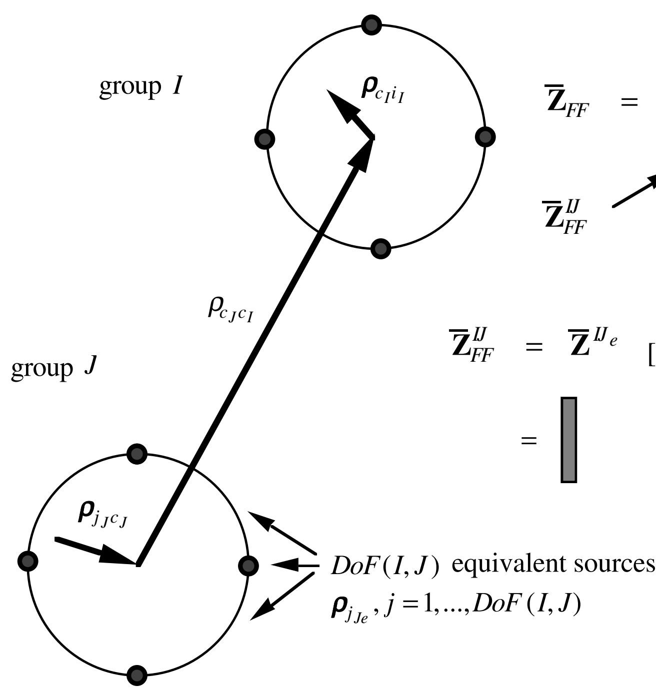

Figure 3. Set of groups (I, J), and MDA-based decomposition of $\overline{\mathbf{Z}}_{FF}^{IJ}$.

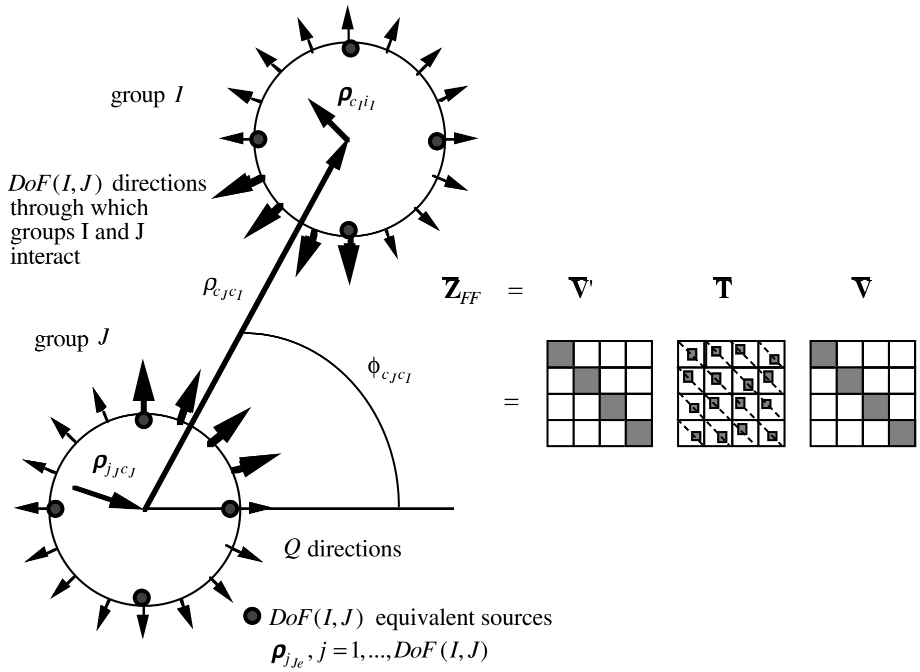

Figure 4. Set of groups (I, J), and FASDPA-based decomposition of $\overline{\mathbf{Z}}_{FF}$. In the FASDPA, the submatrices $\tilde{\overline{\mathbf{T}}}^{IJ}$ are not diagonal but contain a small dense block.

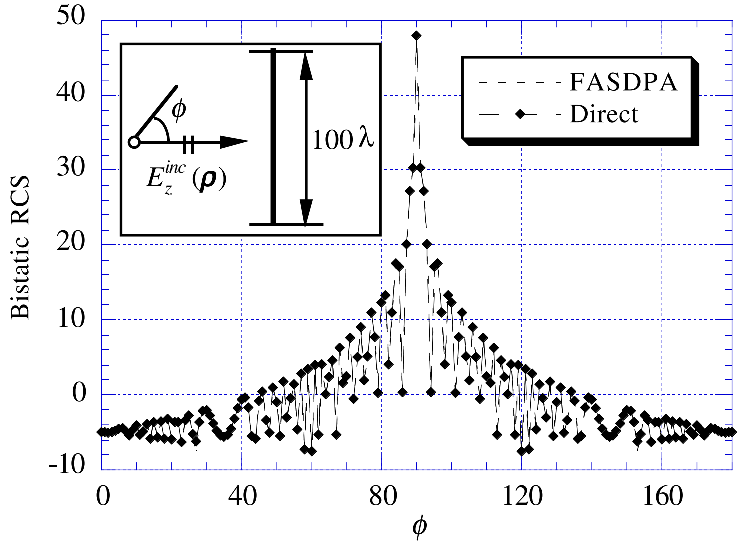

Figure 5. Bistatic RCS of a strip scatterer.

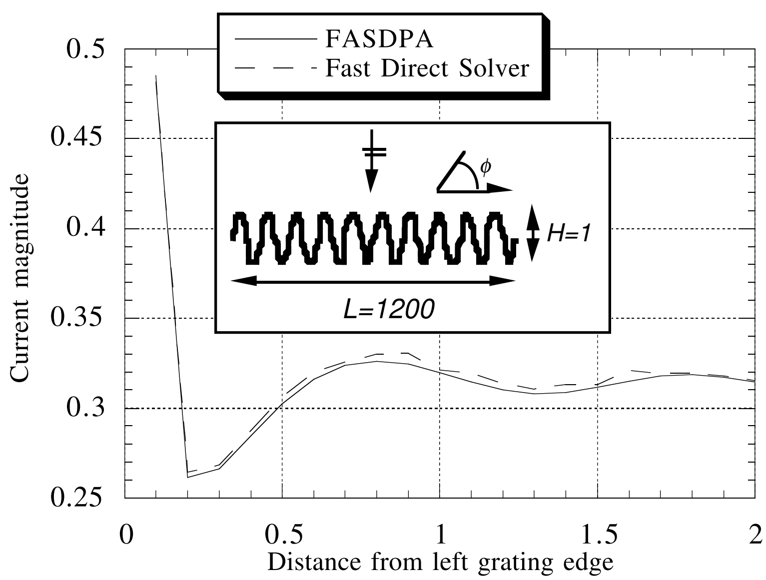

Figure 6. Current on a finite corrugated profile.

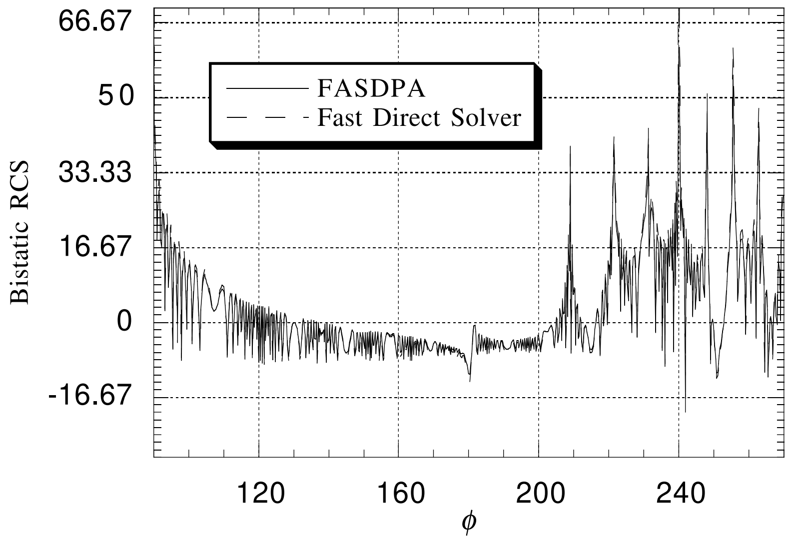

Figure 7. Bistatic RCS of a truncated corrugated profile shown in Figure 6.

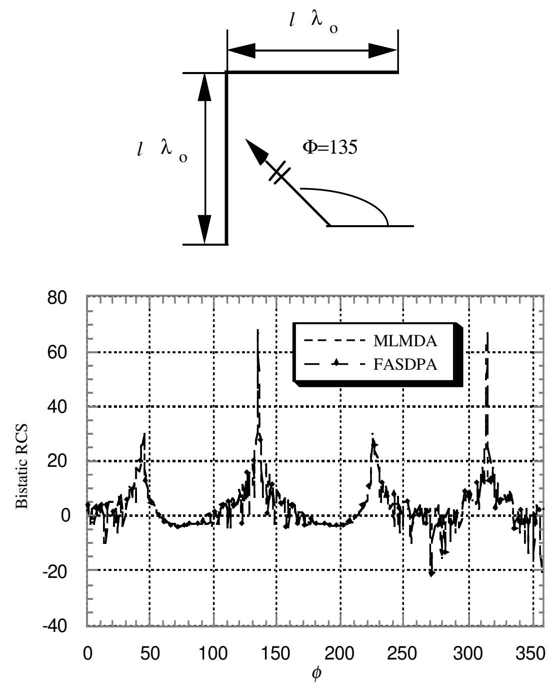

Figure 8. Bistatic RCS of an L-profile.

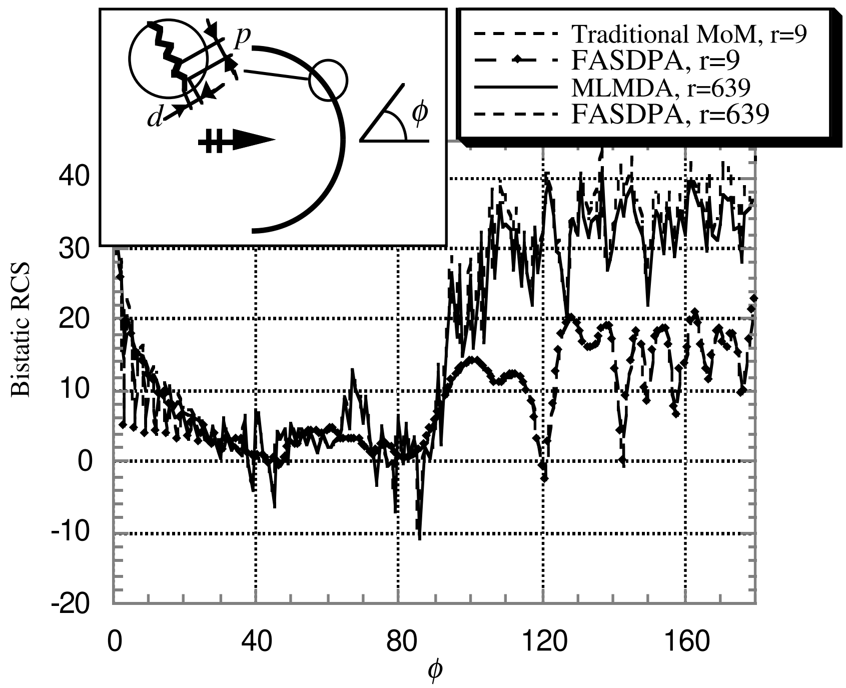

Figure 9. Bistatic RCS of a corrugated semi-circle.

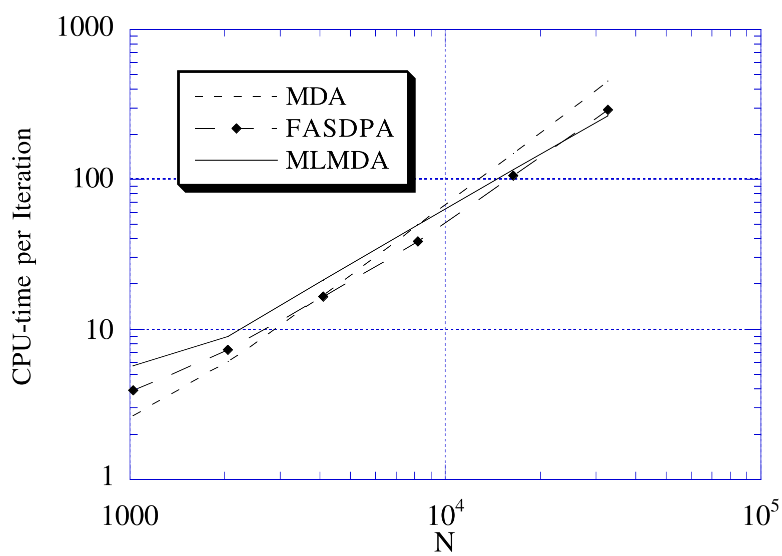

Figure 10. Comparison of CPU-times per iteration for MDA, FASDPA, and MLMDA.